Deep Convolutional Sum-Product Networks

Cory J. Butz
butz@cs.uregina.ca
University of Regina
Canada

Jhonatan S. Oliveira
oliveira@cs.uregina.ca
University of Regina
Canada

André E. dos Santos
dossantos@cs.uregina.ca
University of Regina
Canada

André L. Teixeira
teixeira@cs.uregina.ca
University of Regina
Canada

Abstract

We give conditions under which *convolutional neural networks* (CNNs) define valid *sum-product networks* (SPNs). One subclass, called *convolutional* SPNs (CSPNs), can be implemented using tensors, but also can suffer from being too shallow. Fortunately, tensors can be augmented while maintaining valid SPNs. This yields a larger subclass of CNNs, which we call *deep convolutional* SPNs (DCSPNs), where the convolutional and sum-pooling layers form rich directed acyclic graph structures. One salient feature of DCSPNs is that they are a rigorous probabilistic model. As such, they can exploit multiple kinds of probabilistic reasoning, including *marginal* inference and *most probable explanation* (MPE) inference. This allows an alternative method for learning DCSPNs using vectorized differentiable MPE, which plays a similar role to the generator in *generative adversarial networks* (GANs). Image sampling is yet another application demonstrating the robustness of DCSPNs. Our preliminary results on image sampling are encouraging, since the DCSPN sampled images exhibit variability. Experiments on image completion show that DCSPNs significantly outperform competing methods by achieving several state-of-the-art *mean squared error* (MSE) scores in both left-completion and bottom-completion in benchmark datasets.

Introduction

Generative models are of current interest in the deep learning community, including *generative adversarial networks* (GANs) (Goodfellow et al. 2014), variational autoencoders (Kingma and Welling 2014), neural autoregressive distribution estimators (Larochelle and Murray 2011), pixel recurrent neural networks (Oord, Kalchbrenner, and Kavukcuoglu 2016), and convolutional arithmetic circuits (Sharir et al. 2018). *Convolutional neural networks* (CNNs) (Goodfellow, Bengio, and Courville 2016) can be used in GANs. *Sum-product networks* (SPNs) (Poon and Domingos 2011) are a generative model that have received limited attention from the deep learning community (Peharz et al. 2018). An SPN is a *directed acyclic graph* (DAG), where leaf nodes are tractable distributions and each internal node is either a sum or product operation. A *valid* SPN defines a joint probability distribution and allows for efficient inference (Poon and Domingos 2011).

Conditions are given as to when subclasses of CNNs define valid SPNs, including convolutional layer filters of certain sizes and non-overlapping windows in sum-pooling layers. Satisfaction of these conditions yields a subclass of CNNs, called *convolutional* SPNs (CSPNs). CSPNs permit a vectorized representation allowing for exploitation of tensor libraries such as Tensorflow, but they also can suffer from being too shallow, and it is known that deep SPNs are more expressive than shallow SPNs (Delalleau and Bengio 2011).

We introduce *deep convolutional sum-product networks* (DCSPNs). DCSPNs permit the convolutional and sum-pooling layers to form rich DAG structures by augmenting layer tensors under conditions that maintain *decomposability* and *completeness*. As a decomposable and complete SPN is a valid SPN, our main result is that DCSPNs are a larger subclass of CNNs that define valid SPNs. DCSPNs are a rigorous probabilistic model. As such, they can exploit probabilistic reasoning, including *marginal* inference and *most probable explanation* (MPE) inference. This allows an alternative method for learning DCSPNs using vectorized differentiable MPE. We show how to vectorize MPE using a mask algorithm and how it plays a role similar to the GANs generator. Image sampling is yet another application demonstrating the robustness of DCSPNs. This involves a minor modification to the mask algorithm. Our preliminary results on image sampling are promising, since the DCSPN sampled images exhibit variability. Experimental results on left- and bottom-completion like those in Table 1 show DCSPNs achieve state-of-the-art by building deeper structures using both vertical and horizontal sum-pooling windows, which leverage local structure in the image data in both directions. Applying a simple low pass filter as a post-processing smoothing operation lowers the *mean squared error* (MSE) score from **455** to **401** for left-completion in Olivetti.

Table 1: Mean squared error (MSE) scores in Olivetti Face.

	left	bottom
P&D (Poon and Domingos 2011)	942	918
ICNN (Amos, Xu, and Kolter 2017)	833	-
D&V (Dennis and Ventura 2012)	779	782
DCGAN (Yeh et al. 2017)	935	707
DCSPN	**455**	**503**

Sum-Product Networks

We denote random variables by uppercase letters, such as X and Y, possibly with subscripts, and their values by corresponding lowercase letters x and y. Sets of random variables are denoted by boldfaced uppercase letters and their combined values by corresponding boldfaced lowercase letters.

A *sum-product network* (SPN) (Poon and Domingos 2011) over variables $\mathbf{X}$ can be defined as a *directed acyclic graph* (DAG) containing three types of nodes: leaf distributions, sums, and products. Leaves are tractable distribution functions over $\mathbf{Y} \subseteq \mathbf{X}$. Sum nodes S compute weighted sums $S = \sum_{N \in Ch(S)} w_{S,N} N$, where $Ch(S)$ are the children of S and $w_{S,N}$ are weights that are assumed to be non-negative and normalized (Peharz et al. 2015). Product nodes P compute $P = \prod_{N \in Ch(P)} N$. The value of an SPN, denoted $\mathcal{S}(\mathbf{x})$, is the value of its root.

The *scope* of a sum or product node N is recursively defined as $sc(N) = \bigcup_{C \in Ch(N)} sc(C)$, while the scope of a leaf distribution is the set of variables over which the distribution is defined. A *valid* SPN defines a joint probability distribution and allows for efficient inference (Poon and Domingos 2011). The following two structural constraints on the DAG guarantee validity. An SPN is *complete* if, for every sum node, its children have the same scope. An SPN is *decomposable* if, for every product node, the scopes of its children are pairwise disjoint.

Nodes of an SPN can be organized as layers for a vectorized implementation. The discussion here draws from (Vergari, Di Mauro, and Esposito 2016). The SPN *input layer* is formed by the leaf distribution nodes. Let $\mathbf{L}(\mathbf{x}) \in \mathbb{R}^{\mathbf{s}}$ be the output of a generic layer with s nodes and input $\mathbf{x}$. The value of a *sum layer* with an input $\mathbf{x}$ from r input nodes is

$$\mathbf{L}(\mathbf{x}) = log(\mathbf{w} \times \mathbf{x}), \tag{1}$$

where $\mathbf{w} \in \mathbb{R}^{s \times r}$ is a matrix of weights defining sparse connections:

$$\mathbf{w}_{ij} = \begin{cases} w_{ij} & \text{if edge } (i,j) \text{ exists} \\ 0 & \text{otherwise} \end{cases}$$

and $\mathbf{x} \in [0,1]^r$ represents the input probability values. Similarly, the value of a *product layer* with input $\mathbf{x}$ is

$$\mathbf{L}(\mathbf{x}) = exp(\mathbf{p} \times \mathbf{x}), \tag{2}$$

where $\mathbf{p} \in \{0,1\}^{s \times r}$ is a matrix of sparse connections:

$$\mathbf{p}_{ij} = \begin{cases} 1 & \text{if edge } (i,j) \text{ exists} \\ 0 & \text{otherwise} \end{cases}$$

and $\mathbf{x} \in [0,1]^r$ represents the input probability values in log-space. In this formulation, the exponential and logarithmic functions act as nonlinearities.

In our paper, we relate SPNs with *convolutional neural networks* (CNNs) (Goodfellow, Bengio, and Courville 2016). In general, CNNs are formed by convolutional and pooling layers. A *convolutional layer* can be constructed by applying a convolutional operation with a *filter* on a previous layer output. A *pooling layer* can be built by applying a max or average operation over some elements of the previous layer with respect to a sliding *window*. A sum-pooling layer can be easily obtained from an average-pooling layer.

Convolutional SPNs

We study when subclasses of CNNs define valid SPNs.

First, note that a vectorized SPN can represent a CNN. SPN sum layers correspond to CNN convolutional layers. Here, sum layer weights are convolutional filters and the sum layer value computes the convolution operation. Similarly, SPN product layers correspond to CNN sum-pooling layers. The sum-pooling window computes the product layer value in log-space.

Example 1 *Figure 1 illustrates an SPN with 3 layers being represented by a CNN with 3 layers, where colours represent node scopes. The input layer is the same for both, while the sum and product layers in the SPN are convolutional and sum-pooling layers in the CNN, respectively.*

Conversely, we show how a CNN can represent a vectorized SPN in log-space. Representational, convolutional, and sum-pooling layers in CNNs can represent the input, sum, and product layers in SPNs, respectively.

A *representational layer* (Sharir et al. 2018) is formed by applying n representation functions $f_1, \ldots, f_n : \mathbb{R}^s \to \mathbb{R}$ over s-dimensional local patches of the dataset. We apply the logarithmic function in representational layers so as to correspond to SPN input layers in log-space. For instance, n Gaussian distributions can be used as representation functions to map patches of dataset instances to n values in the representational layer.

The value of a *convolutional layer* with input $\mathbf{x}$ is computed element-wise depending on filter $\mathbf{w}$'s size with depth c being either m-by-n (top) or height-by-width (bottom):

$$\mathbf{L}_{ij}(\mathbf{x}) = \begin{cases} \sum_{q=0}^{m-1} \sum_{l=0}^{n-1} log(\mathbf{w}_{ql}) + \mathbf{x}_{(i+q)(j+l)} \\ \sum_{k=0}^{c-1} log(\mathbf{w}_{ijk}) + \mathbf{x}_{ijk}. \end{cases} \tag{3}$$

Convolutional layers in (3) relate to sum layers in (1).

The value of a *sum-pooling layer* with sliding window size m-by-n and input $\mathbf{x}$ is computed element-wise as:

$$\mathbf{L}_{ij}(\mathbf{x}) = \sum_{q=0}^{m-1} \sum_{l=0}^{n-1} \mathbf{x}_{(i+q)(j+l)}. \tag{4}$$

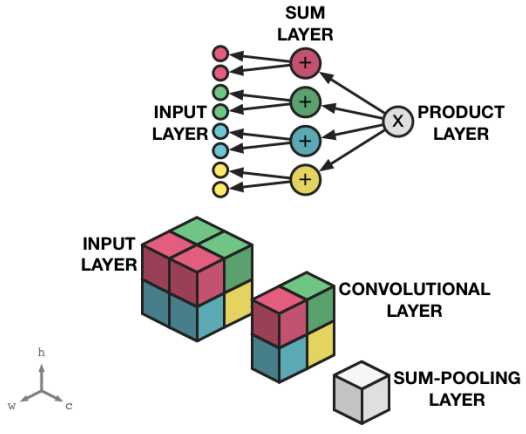

Figure 1: Input, convolutional, and sum-pooling layers in a CNN representing input, sum, and product layers in an SPN.

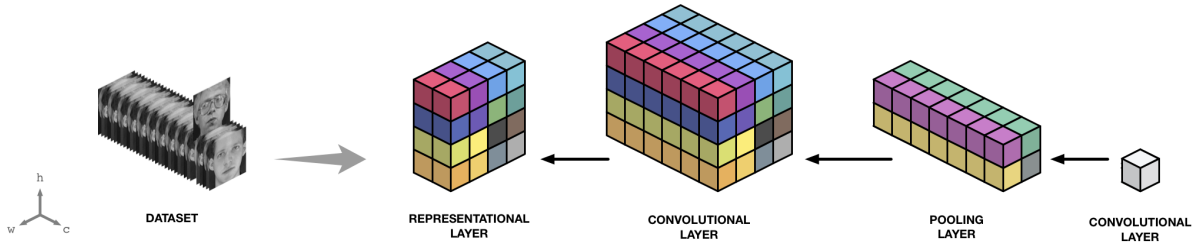

Figure 2: A CSPN represents a valid SPN and is vectorized, but also can suffer from being shallow.

Sum-pooling layers in (4) relate to product layers in (2).

We now define a subclass of CNNs that represent SPNs by restricting convolutional and sum-pooling layers.

Definition 1 *A* convolutional SPN *(CSPN) is a CNN formed under the following two restrictions: (i) convolutional layer filters must have height and width of 1-by-1 or h-by-w, where h and w are the height and width of the convolutional layer, respectively; (ii) in sum-pooling layers, the horizontal and vertical stride of the sliding window must be at least the width and the height of the window itself, respectively.*

Example 2 *Consider the CSPN illustrated in Figure 2, where colours represent node scopes. The dataset is mapped to a 4-by-4 representational layer using 2 representation functions. Next, a convolutional layer is formed with 6 filters of size 4-by-4. A 2-by-2 sum-pooling layer is then built with a 2-by-2 sliding window. Finally, the root node is a 1-by-1 convolutional layer obtained using one 2-by-2 filter.*

Next, we show that CSPNs represent valid SPNs.

Theorem 1 *Let $\mathcal{C}$ be a CSPN formed with respect to a CNN $\mathcal{C}'$ in Definition 1. Then, $\mathcal{C}$ is a* valid *SPN.*

Proof 1 *To be valid, $\mathcal{C}$ must be both* complete *and* decomposable. *The restriction on each convolutional layer filter in $\mathcal{C}'$ to be 1-by-1 or h-by-w ensures that the sum in the convolution operation in (3) occurs over elements of the same scope. Thus, $\mathcal{C}$ is complete. The restriction on the sum-pooling layers with the horizontal and vertical stride of the sliding window being at least the size of the window itself guarantees that the multiplication (summation, in log-space) in the pooling operation in (4) occurs over elements with disjoint scopes in the current and subsequent layers. Therefore, $\mathcal{C}$ is decomposable. By definition, $\mathcal{C}$ is a valid SPN.*

CSPNs can struggle with depth, since the sum-pooling window size quickly reduces the size of the layers. For example, as depicted by the CSPN in Figure 2, the 4-by-4 representational layer reduced to the 1-by-1 root layer after two convolutions and one sum-pooling operation. As deep SPNs are more expressive than shallow SPNs (Delalleau and Bengio 2011), we now turn our attention to introducing deep CSPNs.

We build deep CSPNs by considering two related issues. First, we seek a DAG structure rather than a chain structure. Second, since each node is implemented as a tensor, each combination of tensors must be done such that a valid SPN is maintained. The next section formalizes these ideas.

Deep Convolutional SPNs

In this section, we introduce a tractable generative model, called *deep convolutional SPNs* (DCSPNs).

We denote by $\mathcal{T}$ a tensor of rank (order) n and dimension m in each mode. That is, $\mathcal{T}$ is a multi-dimensional array, specified by a shape with n indexes $[d_1, \ldots, d_n]$, each ranging in $[m] \equiv \{1, \ldots, m\}$. Without loss of generality, a layer is represented as a rank 4 tensor with shape $[b, h, w, c]$, where b is the batch (number of instances) being considered, and h, w, and c are the height, width, and channel (depth), respectively. Tensor elements are SPN nodes. In a sum layer tensor, elements are sum nodes, while in a product layer, tensor elements are product nodes.

Let $\mathcal{T}_1$ and $\mathcal{T}_2$ be two tensors with the same height and the same width. The *channel augmentation* of $\mathcal{T}_1$ and $\mathcal{T}_2$ is the tensor with the same height and the same width formed by concatenating $\mathcal{T}_1$ and $\mathcal{T}_2$ with respect to the channel axis.

Example 3 *Let $\mathcal{T}_1$ and $\mathcal{T}_2$ be the two tensors in Figure 3 (a) (left, right), respectively. Then, the channel augmentation of $\mathcal{T}_1$ and $\mathcal{T}_2$ is the tensor depicted in Figure 3 (b).*

Let $\mathcal{T}_1$ and $\mathcal{T}_2$ be two tensors with the same depth and height. The *width augmentation* of $\mathcal{T}_1$ and $\mathcal{T}_2$ is the tensor with the same depth and the same height formed by concatenating $\mathcal{T}_1$ and $\mathcal{T}_2$ with respect to the width axis. The *height augmentation* is defined similarly.

Example 4 *Let $\mathcal{T}_1$ and $\mathcal{T}_2$ be the two tensors in Figure 3 (c) (left, right), respectively. Then, the width augmentation of $\mathcal{T}_1$ and $\mathcal{T}_2$ is the tensor depicted in Figure 3 (d).*

Definition 2 *A* deep convolutional sum-product network *(DCSPN) $\mathcal{D}$ over n variables $X_1, \ldots, X_n$ is a rooted DAG whose leaves are representational layers and whose internal nodes are convolutional and sum-pooling layers. A convolutional layer with more than one child is formed by recursively applying channel augmentation on all its children. A*

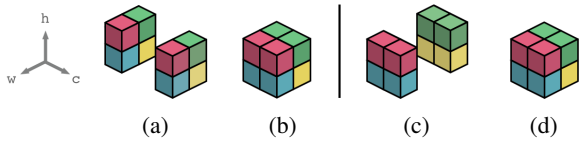

Figure 3: *Channel* (a)-(b) and *width* (c)-(d) augmentations.

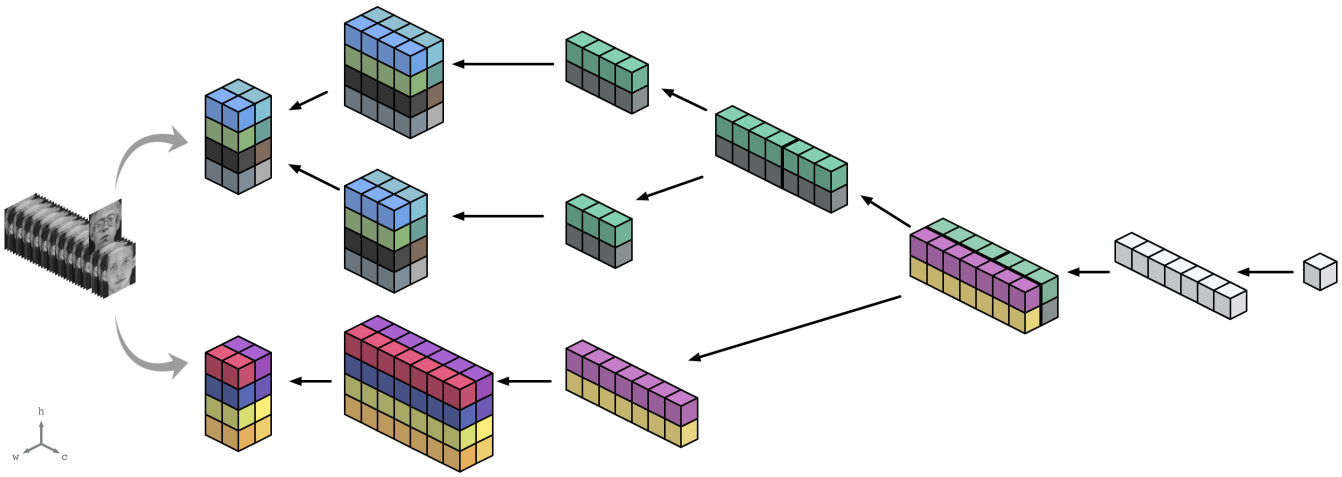

Figure 4: A DCSPN, depicting a rich DAG structure of convolutional and sum-pooling layers, while still being a valid SPN.

sum-pooling layer with more than one child is formed by recursively applying either height or width augmentation on all its children.

Example 5 *Consider the DCSPN in Figure 4. The dataset is mapped to 2 representational layers, each using 2 representation functions. In the upper branches, after a convolutional and a sum-pooling layer, a channel augmentation is used to form a convolutional layer. In the lower branch, after a convolutional and sum-pooling layer, a width augmentation is used to form a sum-pooling layer. Lastly, a sum-pooling layer is followed by the root convolutional layer.*

By construction, DCSPNs represent SPNs. We now provide structural conditions under which DCSPNs represent valid SPNs.

Lemma 1 *Consider a DCSPN $\mathcal{D}$ where every convolutional layer has children over the same element-wise scope. Connect the children of each convolutional layer using channel augmentation. Then, $\mathcal{D}$ is a complete SPN.*

Proof 2 *Consider the SPN defined by the DCSPN $\mathcal{D}$. Channel augmentation over all children of each convolutional layer yields tensors (layers) with elements of the same scope aligned along the channel axis. By construction, summation in the convolutional operation in (3) occurs over the channel axis. Hence, every summation involves operands of the same scope. By definition, $\mathcal{D}$ is complete.*

Lemma 1 is important as it establishes one practical method for combining tensors such that the resulting DCSPN is complete. Lemma 2, given next, provides a practical method for combining tensors such that the obtained DCSPN is decomposable.

Lemma 2 *Consider a DCSPN $\mathcal{D}$ where every sum-pooling layer has children with element-wise disjoint scopes. Connect the children of each sum-pooling layer using either height or width augmentation. Then, $\mathcal{D}$ is a decomposable SPN.*

Proof 3 *Consider the SPN defined by the DCSPN $\mathcal{D}$. Width augmentation over all children of each sum-pooling layer yields tensors (layers) with elements of disjoint scopes at corresponding positions in the width axis. A similar property holds for height augmentation and the height axis. By construction, multiplication in the log-space sum-pooling operation in (4) occurs over either height or width or both axes. Thus, every multiplication involves operands of disjoint scopes. By definition, $\mathcal{D}$ is decomposable.*

We now show the desired result.

Theorem 2 *Let $\mathcal{D}$ be a DCSPN in which the tensors of each convolutional and sum-pooling layer are connected in accordance to Lemmas 1 and 2. Then, $\mathcal{D}$ is a valid SPN.*

Proof 4 *Consider the SPN defined by the DCSPN $\mathcal{D}$. By Lemma 1, $\mathcal{D}$ is necessarily a complete SPN. Moreover, $\mathcal{D}$ is guaranteed to be a decomposable SPN, by Lemma 2. By definition, since $\mathcal{D}$ is both complete and decomposable, $\mathcal{D}$ is a valid SPN.*

Theorem 2 is significant for two reasons. First, as DCSPNs define joint probability distributions, they are tractable deep generative models. Second, DCSPNs are robust in that there are many possible DAG structures in theory satisfying Theorem 2. We will examine later a specific DAG structure that performed exceptionally well in practice.

The DCSPN parameters can be learned with methods such as *expectation maximization* and *gradient descent*, similar to SPNs (Poon and Domingos 2011). More specifically, given a DAG structure, we consider learning its parameters Θ (weights of sum nodes) with the maximum likelihood principle. This optimization problem can be equivalently seen as minimizing the *negative log-likelihood* (NLL) loss function $\mathcal{L}$ (Sharir et al. 2018):

$$\mathcal{L}(\Theta) = \mathbb{E}[-log\ \mathcal{S}(\mathbf{x})]. \tag{5}$$

Given a DCSPN DAG structure coupled with parameters, we turn our attention to applications demonstrating the effectiveness of DCSPNs.

DCSPN Image Completion

Image completion is a difficult task (Dennis and Ventura 2012) that has been studied quite extensively in graphic and vision communities (Poon and Domingos 2011). One SPN approach is to use *most probable explanation* (MPE) inference (Poon and Domingos 2011; Dennis and Ventura 2012). In our case, we will apply MPE inference in CNNs through the unifying framework of DCSPNs.

MPE inference in SPNs is NP-hard (Peharz et al. 2017; Conaty, Mauá, and de Campos 2017). Hence, approximate MPE inference is used (Poon and Domingos 2011; Peharz et al. 2017) and is briefly summarized as two passes. In the forward pass, replace sum nodes with max nodes. The MPE assignment is then obtained via Viterbi-style backtracking. That is, start at the root and follow all children of product nodes and one maximizing child of max nodes.

We propose a method for vectorizing MPE in DCSPNs. In the forward pass, replace the sum operation in a convolutional layer with the max operation. For the backward pass, vectorize the Viterbi-style backtracking by using mask propagation. Starting at the root layer, a tensor mask of all ones initiates the backward propagation. Using a slice of the mask from each parent, a layer computes one mask for its children. Participating children nodes assume value 1; otherwise, 0. Lastly, representational layer masks indicate which representation function is used in the MPE assignment.

Algorithm 1 formally describes our mask MPE backward propagation method, which can utilize sparse tensor optimization techniques available in libraries. Lines 1-2 perform initialization. The DCSPN is traversed according to any topological ordering. For every layer L, we perform two tasks: (i) combine slices from parent masks; and (ii) compute one mask for its children using (i).

Consider task (i). If P is a convolutional layer in line 8, slice the channel (depth) axis at the position of L in the mask from each of its parents. Next, compute the channel augmentation of all slices. Now, suppose P is a sum-pooling layer in line 11, slice the width axis at the position of L in the mask from each of its parents. Observe that here the DAG dictates whether width or height augmentation is applied on all slices. A mask of all ones is used for the root layer. The output of task (i) is the mask PM.

Now consider task (ii). Let L be a convolutional layer in line 18. The activation of L is saved in the forward pass and represents the product of the filter and the input values during the convolution. Determine the position of a maximizing child using the ARGMAX function in line 20. The ONE_HOT function builds a mask of zeros, except for a 1 in the maximizing child position. Lastly, L's mask is the element-wise multiplication of the ONE_HOT mask and PM. Next, if L is a sum-pooling layer, then resize PM in line 24 to match L's previous layer size by upsampling PM using the nearest neighbour method. Lastly, if L is a representational leaf layer, then its mask in line 26 is PM. Finally, return all leaf masks saved in line 26.

The output of Algorithm 1 indicates which representation function is selected in the Viterbi-style backtracking. This, in turn, can be used for computing the MPE assignment of each selected representation function.

Algorithm 1 Mask MPE Backward Propagation

Input: a DCSPN $\mathcal{D}$ with forward pass node values
Output: representational layer leaf masks
Main:

1: **for** L in $\mathcal{D}$ **do** ▷ Initialization
2: $masks[L] = \emptyset$
3: **for** L in TOPOLOGICAL_SORT($\mathcal{D}$) **do**
4: ▷ Task (i): Combine parent layer masks (PM)
5: $PM = \emptyset$
6: **for** P in $Pa(L)$ **do**
7: ▷ Always slice at the position of L
8: **if** P is convolutional **then**
9: $S =$ slice channel axis of $masks[P]$
10: Channel augmentation of PM and S
11: **else** ▷ P is sum-pooling
12: ▷ $\mathcal{D}$ may dictate height augmentation instead
13: $S =$ slice width axis of $masks[P]$
14: Width augmentation of PM and S
15: **if** L is the root **then**
16: $PM = \text{ONES}([1, 1, 1])$
17: ▷ Task (ii): Compute current layer mask (CM)
18: **if** L is convolutional **then**
19: A is the activation of L in the forward pass
20: $C = \text{ARGMAX}(A)$
21: $M = \text{ONE\_HOT}(C)$
22: $mask = M \odot PM$ ▷ Hadamard product
23: **else if** L is sum-pooling **then**
24: $mask = \text{RESIZE}(PM)$ ▷ Upsample
25: **else** ▷ Representational (Leaf)
26: $leaf\_masks[L] = PM$ ▷ Leaf mask
27: $masks[L] = mask$
return $leaf\_masks$ ▷ Masks for leaves of $\mathcal{D}$

Experiments

As promised, we now describe a DCSPN DAG structure that performed exceptionally well in practice. A convolutional layer follows every representational layer and every sum-pooling layer. All convolutional layers have filter sizes height-by-width matching the layer size. Two sum-pooling layers follow each convolutional layer: one with a window size of 1-by-2 and the other 2-by-1. Alternate the window sizes of 1-by-2 and 2-by-1 with 2-by-2 and 2-by-2 every n layers. This hyperparameter n is tuned per dataset and varied between 70 and 100 in our experiments. For each dataset, we randomly set aside one third (up to 50 images) for testing. For training, we use *ADAM* (Kingma and Ba 2014) with a learning rate of 0.005. Four Gaussian representation functions are used per pixel (variable), where the mean and variance are computed from equal quantiles of pixel intensities. In practice, we observed better accuracy when maintaining a sum operation in convolutional layers rather than a max operation during MPE. (Poon and Domingos 2011) made a similar observation.

We compare DCSPNs with *deep convolutional generative adversarial networks* (DCGANs) (Yeh et al. 2017) using the publicly available code from (Amos 2016). Here, we use

the hyperparameter values suggested in (Amos 2016) and 100 epochs during training. The Poisson blending (Pérez, Gangnet, and Blake 2003) post-processing technique for DCGANs is not implemented in (Amos 2016).

Table 1 gives the *mean squared error* (MSE) scores for left-completion and bottom-completion in the *Olivetti* Face dataset (Samaria and Harter 1994). We also compare competing methods in (Poon and Domingos 2011; Amos, Xu, and Kolter 2017; Dennis and Ventura 2012) with DCSPNs. For left-completion, DCSPNs score **455**, which is significantly lower than the next lowest score 779. Similarly, for bottom-completion, DCSPNs (**503**) again dramatically outperform the competition, whose lowest MSE score is 707.

Table 2 shows left-completion and bottom-completion MSE scores in the *Caltech* datasets (Fei-Fei, Fergus, and Perona 2007). (Dennis and Ventura 2012) did not report MSE scores for the Dolphin and Helicopter datasets. DCSPNs have the lowest MSE scores in all three datasets for left-completion. Similarly, for bottom-completion, DCSPNs score well below its competitors in Dolphin and Helicopter, but are slightly edged out by DCGANs in Face. Representative completions are illustrated in Figure 5.

Table 2: MSE scores in Caltech datasets.

left	P&D	D&V	DCGAN	DCSPN
Face	1815	1657	1334	**1178**
Dolphin	3096	-	4096	**2002**
Helicopter	2749	-	3925	**1702**
bottom				
Face	1924	1517	**1046**	1149
Dolphin	2767	-	4016	**2102**
Helicopter	3064	-	3811	**2103**

Analysis suggests several reasons why DCSPNs can reach state-of-the-art results. First, deeper structures are created by simultaneously deriving 1-by-2 and 2-by-1 sum-pooling window sizes. Second, alternating every n layers with window sizes 2-by-2 and 2-by-2 serves as a regularization technique, since larger windows tend to yield shallower DAGs. Third, the known vanishing gradient problem in SPNs (Poon and Domingos 2011) seems to be alleviated by alternating window sizes as above, since this has the effect of creating branches of different lengths. This is similar to how shortcuts work in residual networks (He et al. 2016). Fourth, the vertical and horizontal windows of 1-by-2 and 2-by-1 leverage local structure in the image data in both directions. Fifth, accuracy was improved by using height-by-width instead of a 1-by-1 filter, that is, no sharing of parameters was more effective than sharing parameters. A similar finding was observed in (Sharir et al. 2018).

Figure 5: Columns show original, DCSPN, DCGAN, and P&D. The first and second rows show left-completion and bottom-completions, respectively. Left and right pictures are from datasets Olivetti Face and Caltech Face, respectively.

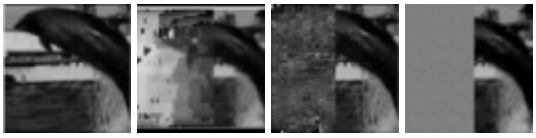

(a) (b) (c) (d)

Figure 6: DCSPNs performed well on a dataset with 65 images. Left-completion of the original image in (a) by DCSPN (b), P&D (c), and DCGAN (d).

DCSPNs left-complete well on a small dataset. The Caltech Dolphin dataset only contains 65 images. Nevertheless, DCSPNs performed quite well, as exemplified by the MSE scores in Table 2 and by the left-completions illustrated in Figure 6.

On the contrary, DCSPN completions admittedly look as though they are sometimes composed of random blocks of high frequency. To mitigate this, a low pass Gaussian filter can be applied as a smoothing post-processing step. This simple technique lowers the DCSPN MSE score in Olivetti left-completion in Table 1 from 455 to **401**.

We also tried other common CNN techniques, such as average-pooling instead of sum-pooling layers, sharing parameters in convolutional layers, batch normalization, and dropout, but did not observe any significant improvement. It is noted that dropout was successfully applied in SPNs for image classification (Peharz et al. 2018).

DCSPNs with Differentiable MPE

Motivated by future work suggested in (Vergari et al. 2018), we propose an alternative method of training DCSPNs that is based on differentiable MPE. Whereas (5) minimizes the negative log-likelihood loss function, the new training method also considers the error between the given input and the MPE assignment (completion).

More formally, let $D(\mathbf{x})$ be the value of a DCSPN $\mathcal{D}$ with input $\mathbf{x}$. Let $\mathbf{Y} \subseteq \mathbf{X}$ and consider input $\mathbf{y}$, where the value of each variable in $\mathbf{Y}$ is 1, namely, the variables in $\mathbf{Y}$ are marginalized out. The MPE assignment after both forward and backward propagation in $\mathcal{D}$ is denoted by $M(\mathbf{y})$. Then, the objective function for training $\mathcal{D}$ can be defined as:

$$\min_{M} \max_{D} \mathbb{E}[log\ D(\mathbf{x})] + \mathbb{E}[log(1 - D(M(\mathbf{y})))]. \qquad (6)$$

Using (6) to train DCSPNs yields an MSE score of **651** for left-completion in the Olivetti dataset. This beats all competing scores in Table 1, except for DCSPNs trained using (5). Training DCSPNs using (6) is intriguing for more than simply a promising MSE score.

The training in (6) is similar to GANs training, which, in general, involves two networks: a generator $\mathcal{G}$ and a discriminator $\mathcal{D}$. The input to $\mathcal{G}$ is a random sample $\mathbf{z}$ drawn from

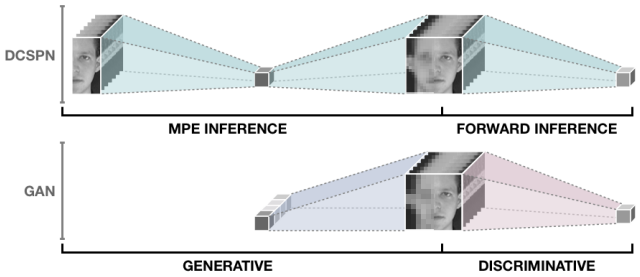

Figure 7: MPE and forward inference in SPNs are similar to the generator and discriminator in GANs, respectively.

a simple distribution such as a normal distribution. $\mathcal{G}$ upsamples $\mathbf{z}$ and outputs $G(\mathbf{z})$. The discriminator $\mathcal{D}$ receives $G(\mathbf{z})$ or dataset samples $\mathbf{x}$ and downsamples to a classification output. Hence, training GANs involves minimizing G and maximizing D:

$$\min_G \max_D \mathbb{E}[log\ D(\mathbf{x})] + \mathbb{E}[log(1 - D(G(\mathbf{z})))]. \tag{7}$$

Figure 7 illustrates a general relationship between training DCSPNs with differentiable MPE in (6) and GANs training in (7). Observe that MPE inference computing $M(\mathbf{y})$ in (6) plays the role of the generator $\mathcal{G}$ in GANs computing $G(\mathbf{z})$ in (7). However, while the GANs generator $\mathcal{G}$ upsamples noise to form an image, DCSPNs use MPE inference to upsample the network value to form an image.

Similarly, forward inference in DCSPNs computing $D(\mathbf{x})$ in (6) assumes the part of the discriminator in GANs computing $D(\mathbf{x})$ in (7). Hence, DCSPN forward inference downsamples to a log-likelihood value measuring how likely the given input is from the sample distribution, whereas the GANs discriminator downsamples to a classification of whether or not the input data is real.

On the other hand, the GANs generator has its own learnable parameters, since the generator and discriminator are two different networks. However, a DCSPN is a single network, resulting in the sharing of parameters during learning between MPE inference and forward inference. Further investigation of DCSPNs with differentiable MPE and its relationship to GANs training remains as future work.

Image Sampling

DCSPNs can sample images by modifying Algorithm 1. Instead of selecting a maximizing child, randomly select a child. More formally, replace lines 19 and 20 to instead assign values to C by randomly sampling from a categorical distribution parameterized by the convolutional layer filter weights. Note that the forward pass is no longer needed.

The sampled images in Figure 8 are encouraging as variability is evident. Moreover, these results were obtained in an inaugural attempt at DCSPN image sampling involving a minor modification to Algorithm 1. Some generative models, including GANs, are known for low variability due to *mode collapse* (Metz et al. 2017; Salimans et al. 2016).

Figure 8: DCSPN image sampling shows variability.

Related Works

Here we comment on other vectorized approaches to SPNs.

(Poon and Domingos 2011) and (Vergari, Di Mauro, and Esposito 2015) have discussed relationships between CNNs and SPNs. The interpretation of an SPN sum layer depends on the type of probabilistic inference being conducted. For marginal inference, an SPN sum layer corresponds to a convolutional layer in CNNs. For MPE, on the other hand, an SPN sum layer corresponds to a max-pooling layer in CNNs. We extend the literature by showing that an SPN product layer can correspond to a sum-pooling layer in CNNs.

(Sharir et al. 2018) introduced a tractable generative model, called *convolutional arithmetic circuits* (ConvACs). An *arithmetic circuit* (Darwiche 2003) is a deep learning model that has been shown by (Rooshenas and Lowd 2014) to be equivalent to SPNs. In particular, ConvACs include a *representation layer* (Sharir et al. 2018). We found this introduction useful in practice. However, similar to CSPNs, ConvACs may suffer from being shallow.

(Peharz et al. 2018) suggest an SPN learning method involving a discriminative and generative loss function. Although the generative part is also based on the log-likelihood similar to (6), the discriminative part is different. They consider the cross-entropy function of the SPN parameters, while we introduced to notion of a minmax game using differentiable MPE.

Conclusion

Deep convolutional sum-product networks (DCSPNs) can form rich DAG structures of convolutional and sum-pooling layers, while still being valid SPNs. As a tractable generative model, DCSPNs can perform efficient probabilistic reasoning, including marginal inference and approximate MPE inference. On the other hand, as a CNN, DCSPNs can build deeper structures using both vertical and horizontal sum-pooling windows, which leverage local structure in the image data. Practical applications of DCSPNs include image completion and image sampling. DCSPNs are flexible in that they allow for an alternative learning method based on differentiable MPE. Relationships between this learning approach and learning in GANs are discussed.

Experimental results show that DCSPNs significantly outperform competitors and achieve several state-of-the-art results. For example, Table 1 reports the MSE scores for image left-completion in the benchmark Olivetti Face dataset. The DCSPN score of **455** is well below the next lowest score of 779 obtained in (Dennis and Ventura 2012). Applying a simple low pass filter as a post-processing step lowers the DCSPN MSE score down to **401**.

References

Amos, B.; Xu, L.; and Kolter, J. Z. 2017. Input convex neural networks. In *Proceedings of the Thirty-Fourth International Conference on Machine Learning (ICML 2017)*.

Amos, B. 2016. Image Completion with Deep Learning in TensorFlow. http://bamos.github.io/2016/08/09/deep-completion. Accessed: July 1st, 2018.

Conaty, D.; Mauá, D.; and de Campos, C. P. 2017. Approximation complexity of maximum a posteriori inference in sum-product networks. In *Proceedings of the Thirtieth Conference on Uncertainty in Artificial Intelligence (UAI 2017)*.

Darwiche, A. 2003. A differential approach to inference in Bayesian networks. *Journal of the ACM (JACM)* 50(3):280–305.

Delalleau, O., and Bengio, Y. 2011. Shallow vs. deep sum-product networks. In *Proceedings of the Twenty-Fourth Conference on Neural Information Processing Systems (NIPS 2011)*, 666–674.

Dennis, A., and Ventura, D. 2012. Learning the architecture of sum-product networks using clustering on variables. In *Proceedings of the Twenty-Fifth Conference on Neural Information Processing Systems (NIPS 2012)*, 2033–2041.

Fei-Fei, L.; Fergus, R.; and Perona, P. 2007. Learning generative visual models from few training examples: An incremental Bayesian approach tested on 101 object categories. *Computer Vision and Image Understanding* 106(1):59–70.

Goodfellow, I.; Bengio, Y.; and Courville, A. 2016. *Deep Learning*. MIT Press.

Goodfellow, I.; Pouget-Abadie, J.; Mirza, M.; Xu, B.; Warde-Farley, D.; Ozair, S.; Courville, A.; and Bengio, Y. 2014. Generative adversarial nets. In *Proceedings of the Twenty-Seventh Conference on Neural Information Processing Systems (NIPS 2014)*, 2672–2680.

He, K.; Zhang, X.; Ren, S.; and Sun, J. 2016. Deep residual learning for image recognition. In *Proceedings of the IEEE Conference on Computer Vision and Pattern Recognition (CVPR 2016)*, 770–778.

Kingma, D. P., and Ba, J. 2014. Adam: A method for stochastic optimization. *arXiv preprint arXiv:1412.6980*.

Kingma, D. P., and Welling, M. 2014. Auto-encoding variational Bayes. In *Proceedings of the International Conference on Learning Representations (ICLR 2014)*.

Larochelle, H., and Murray, I. 2011. The neural autoregressive distribution estimator. In *Proceedings of the Fourteenth International Conference on Artificial Intelligence and Statistics (AISTATS 2011)*, 29–37.

Metz, L.; Poole, B.; Pfau, D.; and Sohl-Dickstein, J. 2017. Unrolled generative adversarial networks. *Proceedings of the International Conference on Learning Representations (ICLR 2017)*.

Oord, A. v. d.; Kalchbrenner, N.; and Kavukcuoglu, K. 2016. Pixel recurrent neural networks. In *Proceedings of the International Conference on Machine Learning (ICML 2016)*.

Peharz, R.; Tschiatschek, S.; Pernkopf, F.; and Domingos, P. 2015. On theoretical properties of sum-product networks. In *Proceedings of the Eighteenth International Conference on Artificial Intelligence and Statistics (AISTATS 2015)*, 744–752.

Peharz, R.; Gens, R.; Pernkopf, F.; and Domingos, P. 2017. On the latent variable interpretation in sum-product networks. *IEEE Transactions on Pattern Analysis and Machine Intelligence* 39(10):2030–2044.

Peharz, R.; Vergari, A.; Stelzner, K.; Molina, A.; Trapp, M.; Kersting, K.; and Ghahramani, Z. 2018. Probabilistic deep learning using random sum-product networks. *arXiv preprint arXiv:1806.01910*.

Pérez, P.; Gangnet, M.; and Blake, A. 2003. Poisson image editing. *ACM Transactions on Graphics (TOG)* 22(3):313–318.

Poon, H., and Domingos, P. 2011. Sum-product networks: A new deep architecture. In *Proceedings of the Twenty-Seventh Conference on Uncertainty in Artificial Intelligence (UAI 2011)*, 337–346.

Rooshenas, A., and Lowd, D. 2014. Learning sum-product networks with direct and indirect variable interactions. In *Proceedings of the Thirty-First International Conference on Machine Learning*, 710–718.

Salimans, T.; Goodfellow, I.; Zaremba, W.; Cheung, V.; Radford, A.; and Chen, X. 2016. Improved techniques for training gans. In *Proceedings of the Thirtieth Annual Conference on Neural Information Processing Systems (NIPS 2016)*, 2234–2242.

Samaria, F. S., and Harter, A. C. 1994. Parameterisation of a stochastic model for human face identification. In *Proceedings of the Second IEEE Workshop on Applications of Computer Vision (WACV 1994)*, 138–142.

Sharir, O.; Tamari, R.; Cohen, N.; and Shashua, A. 2018. Tensorial mixture models. *arXiv preprint arXiv:1610.04167*.

Vergari, A.; Peharz, R.; Di Mauro, N.; Molina, A.; Kersting, K.; and Esposito, F. 2018. Sum-product autoencoding: Encoding and decoding representations using sum-product networks. In *Proceedings of the Thirty-Second AAAI Conference on Artificial Intelligence (AAAI 2018)*, 4163–4170.

Vergari, A.; Di Mauro, N.; and Esposito, F. 2015. Simplifying, regularizing and strengthening sum-product network structure learning. In *Proceedings of the Joint European Conference on Machine Learning and Knowledge Discovery in Databases (ECML PKDD 2015)*, 343–358.

Vergari, A.; Di Mauro, N.; and Esposito, F. 2016. Visualizing and understanding sum-product networks. *arXiv preprint arXiv:1608.08266*.

Yeh, R. A.; Chen, C.; Lim, T. Y.; Schwing, A. G.; Hasegawa-Johnson, M.; and Do, M. N. 2017. Semantic image inpainting with deep generative models. In *Proceedings of the IEEE Conference on Computer Vision and Pattern Recognition (CVPR 2017)*, 6882–6890.